J. Fluid Mech. (2000), *vol.* 404, *pp.* 289–309. Printed in the United Kingdom

Reynolds-number-independent instability of the boundary layer over a flat surface: optimal perturbations

By PAOLO LUCHINI

Dipartimento di Ingegneria Aerospaziale, Politecnico di Milano, Via La Masa 34, 20158 Milano, Italy

(Received 26 June 1997 and in revised form 4 October 1999)

The dependence on initial conditions of the three-dimensional algebraic spatial instability of the Blasius boundary layer is examined by a recently developed method of receptivity analysis based on the upstream integration of adjoint equations. This method allows us to determine optimal perturbations, i.e. initial perturbations that maximize the energy growth, even in the wavenumber range where the problem is not amenable to a mode analysis, and thus to complement a previous paper in which the small-wavenumber regime was described.

1. Introduction

Ellingsen & Palm (1975) and Landahl (1980) identified a new disturbance amplification mechanism, according to which a low-amplitude longitudinal vortex superposed on an otherwise two-dimensional boundary layer can lift up low-velocity fluid from the wall and push down high-velocity fluid towards the wall. The structure of the boundary layer being elongated, with a typical size in the streamwise direction $R^{1/2}$ times greater than its thickness, the accumulated longitudinal-velocity disturbance can be $O(R^{1/2})$ times greater than the crossflow disturbance from which it originated (where R denotes the longitudinal Reynolds number). A phenomenon driven by the same mechanism was explained a decade earlier by Crow (1966), who studied linearly growing perturbations induced in a boundary layer by a spanwise oscillation of the outer stream; at the time, however, the process could not be seen as one of energy amplification because the energy of the outer stream is infinite.

The combination of this basically inviscid amplification mechanism with the damping effect of viscosity produces the phenomenon that was eventually named 'transient growth' (e.g. Hultgren & Gustavsson 1981; Gustavsson 1991; Lundbladh & Johansson 1991; Butler & Farrell 1992; Reddy & Henningson 1993; Henningson, Lundbladh & Johansson 1993; Trefethen, *et al.* 1993; Bagget, Driscoll & Trefethen 1995). This mechanism is believed to be at the origin of the Klebanoff modes (Klebanoff, Tidstrom & Sargent 1962) giving rise to the so-called bypass transition (Morkovin 1968, 1984, Morkovin & Reshotko 1990). Gebhardt & Grossmann (1994), and Bagget & Trefethen (1997) have additionally shown, in the context of low-dimensional model equations, that the same algebraic growth mechanism is also capable of amplifying the quasi-steady beat produced by the quadratic self-interaction of high-frequency disturbances. Boberg & Brosa (1988) and, more recently, Hamilton, Kim & Waleffe (1995) have proposed a similar linear amplification mechanism as being responsible for the transfer of energy from the mean flow to vortical structures in developed turbulence.

The receptivity of a boundary layer to small-amplitude streamwise vortices convected downstream by the impinging current, on the other hand, was studied by Luchini (1996). He showed that, in the limit of small spanwise wavenumber, viscous damping in a spatially growing boundary layer is insufficient to terminate the algebraic growth induced by such disturbances. In this limit a similarity solution of the linearized boundary layer equations (an extension to three dimensions of the two-dimensional solution studied by Libby & Fox in 1964) describes the spatially growing perturbation caused by a spanwise-periodic steady longitudinal vortex.

The assumption of small spanwise wavenumber, however, impeded us in determining the wavenumber for which amplification is a maximum, because the approximation used, being a first-order perturbation expansion in wavenumber, can only provide an amplification that increases linearly with wavenumber itself. The approximation fails for wavenumbers of the order of the reciprocal of the boundary layer thickness, and all that could be said is that the maximum should be expected to fall in a neighbourhood of this value.

The present paper constitutes a continuation of Luchini (1996, subsequently referred to as L96), and sets out to determine the maximum available amplification and the corresponding wavenumber and perturbation velocity profile. A rigorous definition of the maximum is achieved through the concept of optimal perturbation, as introduced by Boberg & Brosa (1988) and Butler & Farrell (1992).

It should be mentioned that after the first submission of this paper a number of related approaches have been presented at conferences and/or in journals. Most notably Andersson, Berggren & Henningson (1998*a*, *b*, *c*; 1999*a*, *b*, *c*, *d*) have calculated the optimal perturbations of a flat-plate boundary layer by an adjoint-based optimization technique similar to the one presented herein. Similarities and differences between their work and ours will be discussed in the conclusion.

2. The definition and iterative determination of optimal perturbations

We shall take as our starting mathematical model the linearized three-dimensional boundary-layer equations:

$$\delta u_x + \delta v_y + \mathrm{i}\alpha\delta w = 0, \tag{1a}$$

$$-\mathrm{i}\omega\delta u + u_0\delta u_x + v_0\delta u_y + u_{0,x}\delta u + u_{0,y}\delta v = \delta u_{yy} - \alpha^2\delta u, \tag{1b}$$

$$-\mathrm{i}\omega\delta v + u_0\delta v_x + v_0\delta v_y + v_{0,x}\delta u + v_{0,y}\delta v + \delta p_y = \delta v_{yy} - \alpha^2\delta v, \tag{1c}$$

$$-\mathrm{i}\omega\delta w + u_0\delta w_x + v_0\delta w_y + \mathrm{i}\alpha\delta p = \delta w_{yy} - \alpha^2\delta w, \tag{1d}$$

which for steady perturbations become the same as equations (8) of L96. The relevant boundary conditions are: $\delta u = \delta v = \delta w = 0$ at the wall, where $y = 0$, and $\delta u = \delta w = \delta p = 0$ for $y \to \infty$. Coordinates are made dimensionless with a reference length L in the x-direction and $d = R^{-1/2}L$ in the y- and z-directions; U_∞ is the reference velocity for the u-component and $R^{-1/2}U_\infty$ is the reference velocity for the v- and w-components. The Reynolds number is defined as $R = U_\infty L/\nu$. The unperturbed velocity components $u_0(x, y)$ and $v_0(x, y)$ are obtained from Blasius' similarity solution for the two-dimensional boundary layer over a flat plate. The disturbance is assumed to be sinusoidally varying in the z-direction and in time as $\mathrm{e}^{\mathrm{i}\alpha z - \mathrm{i}\omega t}$. For the justification and discussion of the range of applicability of (1) the reader is referred to L96. In the unsteady case it need only be added that the frequency ω, made dimensionless with respect to L/U_∞, must not be exceedingly large compared to unity in order to preserve the validity of the boundary layer approximation. However, to simplify the

exposition we may anticipate the result that the maximum amplification is found for $\omega = 0$, as is generally true of algebraic instabilities based on the lift-up mechanism of Landahl (1980). In fact, the gradual accumulation of small induced longitudinal-velocity disturbances, necessary to produce a sizeable streak, is generally hampered by oscillations of changing sign that tend to cancel each other.

If the linearized boundary layer is viewed in black-box fashion as an amplifier of velocity perturbations applied at its input, it makes sense to ask what maximum ratio of output to input energy this amplifier can provide and which shape of the oncoming perturbation the maximum corresponds to. This question was answered for the temporal stability of pipe flow by Boberg & Brosa (1988), and for plane parallel flows (including boundary layers treated as parallel flows) by Butler & Farrell (1992), who introduced the term 'optimal perturbation' to denote the input velocity profile giving rise to maximum amplification of the disturbance energy. They were thus able to observe that the optimal perturbations can be totally different from the eigenfunctions of the linear stability problem, and the maximum gain can be positive even when all the eigenvalues have negative real parts. They found optimal perturbations in the general appearance of longitudinal vortices and induced disturbances in the general appearance of longitudinal streaks, thus confirming the lift-up amplification mechanism initially proposed by Ellingsen & Palm (1975) and Landahl (1980).

From a mathematical viewpoint, the optimization of a fluid dynamics perturbation is no different from any other linear optimization problem. In terms of the input–output operator $\mathbf{U}$ acting on a yet unspecified state vector $\boldsymbol{f}$ of the system (or of its matrix representation in discretized form), the maximum gain is the operator's norm, namely†

$$g_{opt} = \max_{\boldsymbol{f}} \frac{|\mathbf{U}\cdot\boldsymbol{f}|^2}{|\boldsymbol{f}|^2} = \max_{\boldsymbol{f}} \frac{\boldsymbol{f}^*\cdot\mathbf{U}^+\cdot\mathbf{U}\cdot\boldsymbol{f}}{\boldsymbol{f}^*\cdot\boldsymbol{f}}\,, \tag{2}$$

and is also the largest singular value of this operator or matrix, whereas the optimal perturbation is given by the corresponding singular vector, i.e. the corresponding eigenvector of $\mathbf{U}^+\cdot\mathbf{U} = \mathbf{U}^{T*}\cdot\mathbf{U}$. Equation (2) represents the Rayleigh quotient generated by the positive-definite Hermitian operator $\mathbf{U}^+\cdot\mathbf{U}$ (which turns out to be just a real symmetric operator for steady disturbances, because in this case (1) can be recast into a form with all real coefficients by taking $\mathrm{i}\delta w$ as a new variable). As is known from matrix algebra, the maximum and minimum of g occur in correspondence with eigenfunctions of this operator, i.e. functions such that

$$\mathbf{U}^+\cdot\mathbf{U}\cdot\boldsymbol{f} = g\boldsymbol{f}. \tag{3}$$

Moreover, since all singular values are real and positive, a simple direct-iteration algorithm of the form

$$\boldsymbol{f}_{n+1} = \mathbf{U}^+\cdot\mathbf{U}\cdot\boldsymbol{f}_n \tag{4}$$

always converges to the optimal perturbation, the one corresponding to maximum gain in perturbation energy. As can be seen from (3), once $\boldsymbol{f}_{n+1}$ has become, for n large enough, proportional to $\boldsymbol{f}_n$, the proportionality ratio between them gives the singular value g itself.

In what follows we shall need a slight generalization of the above classical result, to a situation in which the input and output energies are expressed by two, arbitrary

† The following notational conventions are adopted: a $*$ superscript denotes complex conjugate, a $+$ superscript denotes adjoint (conjugate transposed), and a dot product stands for bare index contraction without any complex conjugation implied.

and possibly different, positive-definite quadratic forms $E_{in} = \boldsymbol{f}^* \cdot \mathbf{Q}_{in} \cdot \boldsymbol{f}$ and $E_{out} = \boldsymbol{f}^* \cdot \mathbf{Q}_{out} \cdot \boldsymbol{f}$, so that the gain to be maximized is given by

$$g = (\boldsymbol{f}^* \cdot \mathbf{U}^+ \cdot \mathbf{Q}_{out} \cdot \mathbf{U} \cdot \boldsymbol{f})/(\boldsymbol{f}^* \cdot \mathbf{Q}_{in} \cdot \boldsymbol{f}). \tag{5}$$

In such a case, on giving an arbitrary variation δf to f and imposing that the ensuing δg should vanish, we find the extremality condition that

$$\mathbf{U}^+ \cdot \mathbf{Q}_{out} \cdot \mathbf{U} \cdot \boldsymbol{f} = g \mathbf{Q}_{in} \cdot \boldsymbol{f}. \tag{6}$$

The corresponding direct-iteration algorithm, analogous to (4), becomes

$$\boldsymbol{f}_{n+1} = \mathbf{Q}_{in}^{-1} \cdot \mathbf{U}^+ \cdot \mathbf{Q}_{out} \cdot \mathbf{U} \cdot \boldsymbol{f}_n. \tag{7}$$

3. Numerical determination of the optimal disturbances by the method of adjoint equations

As observed in the previous section, it is a mathematically straightforward task to determine the optimal perturbation and maximum gain whenever a numerical approximation of the operator $\mathbf{U}$ can be assigned in matrix form. For instance, Butler & Farrell (1992), in order to study the temporal instability of a parallel flow, projected the perturbation over the set of eigenfunctions of the time-independent perturbation equations and calculated a matrix representation of the input–output transfer operator with respect to this basis.

However, when an evolving base flow is considered, as in the present problem of the spatial instability of a boundary layer, the concept of local eigenfunctions loses meaning in general. (There are particular cases where it can be recovered in a suitable asymptotic sense, though. For instance, in the limit of small spanwise wavenumber as in L96, or in the limit of large longitudinal wavenumber as in the classical theory of Tollmien–Schlichting waves.) If local eigenfunctions are excluded, the only remaining possibility seems to be that of calculating a numerical approximation of the transfer operator $\mathbf{U}$ by expanding the initial condition in a set of more or less arbitrary base functions, and performing repeated numerical solutions of (1) in each of which the initial condition is given as one of the base functions. This represents an amount of computational work which, although not unaffordable, is much larger than the work involved in the non-evolving case, where an analytical solution was available.

A much more effective and flexible technique is known in the general mathematical theory of optimal control: the simultaneous use of direct and adjoint equations. The system of differential equations adjoint to (1) was numerically solved for a different but related purpose (the calculation of the receptivity of Görtler vortices) by Luchini & Bottaro (1996, 1998, subsequently referred to as LB). They found that a *backward-in-time* integration of the adjoint system requires very nearly the same computer time as a forward integration of the direct system.

The availability of a quick numerical integration of the adjoint system makes the iterative algorithm of (4) or (7) an appealing alternative to the explicit determination of a matrix representation of the operator $\mathbf{U}$. In fact, the product $\mathbf{U} \cdot \boldsymbol{f}_n$, representing the output of an individual numerical simulation performed with initial condition $\boldsymbol{f}_n$, is computationally much faster to obtain than a discrete approximation of $\mathbf{U}$ itself. Once $\mathbf{U} \cdot \boldsymbol{f}_n$ is calculated and multiplied by $\mathbf{Q}_{out}$, the final multiplication by $\mathbf{U}^+$ to give $\mathbf{U}^+ \cdot (\mathbf{Q}_{out} \cdot \mathbf{U} \cdot \boldsymbol{f}_n)$ can then be obtained through the algorithm of LB in about the same computational time again, for this product represents the output of a *backward* (i.e. marching upstream) numerical integration of the adjoint differential problem with

initial condition $\mathbf{Q}_{out} \cdot \mathbf{U} \cdot \boldsymbol{f}_n$. Therefore, a single iteration of (7) costs just as much as two numerical integrations of the original system of equations (1); provided the maximization converges in less than $N/2$ iterations, where N is the number of degrees of freedom in the numerical discretization of the input condition, the algorithm is faster than calculating a matrix representation of $\mathbf{U}$.

To summarize, the algorithm we have adopted for determining the optimal initial conditions is composed of four steps, each corresponding to one of the four operators in (7):

Step $\mathbf{U}$: forward numerical integration of the parabolic system of differential equations (1) from the input cross-section $x_{in} = 0^-$ (immediately upstream of the sharp leading edge where the boundary layer is formed) to the output cross-section $x_{out} = 1$ (the distance from the leading edge to the output cross-section having been assumed as the reference length L).

Step $\mathbf{Q}_{out}$: multiplication of the output disturbance profile just obtained by the energy matrix $\mathbf{Q}_{out}$ to give the initial condition for the next step.

Step $\mathbf{U}^+$: backward numerical integration of the backward-parabolic adjoint system of differential equations from x_{out} to x_{in}, to give the receptivity to initial disturbances.

Step $\mathbf{Q}_{in}$: multiplication of the initial receptivity by $\mathbf{Q}_{in}^{-1}$ to give the next approximation of the optimal disturbance, which is then normalized to prevent floating-point overflow and fed back to step $\mathbf{U}$.

The loop is initiated with an arbitrary disturbance profile, and repeated until calculated variations in the profile itself become negligible. As will be discussed in greater detail later, convergence turned out to be extremely fast.

4. Properties of the boundary-layer model

As the boundary-layer equations (1) are the same as generally adopted, with the addition of a centrifugal-force term, to model Görtler vortices, the algorithm for the integration of the direct and adjoint equations could be obtained from the one described in LB by simply setting the centrifugal force (i.e. the wall's curvature) equal to zero. Therefore, the details of the numerical implementation of the $\mathbf{U}$ and $\mathbf{U}^+$ steps of (7) can be found in LB, and we just briefly recall the main properties of (1) here.

Unlike the Navier–Stokes equations they are meant to approximate, the boundary-layer equations are parabolic rather than elliptic, and require two rather than three initial conditions at $x = x_{in}$ and none at $x = x_{out}$. In addition, the coefficients of these equations are singular at $x = 0$, the edge of the plate, where the v_0-component of the base flow is infinite for $x \to 0^+$ (from the right), and is identically zero for $x \to 0^-$ (from the left). As all this implies, the boundary-layer equations are not uniformly valid in a neighbourhood of $x = 0$, and jump conditions are needed to connect the velocity disturbances at $x = 0^+$ with those at $x = 0^-$.

The description of the leading-edge region adopted by LB (and previously, for a different purpose, by Ting 1965) is based on the following ideas:

(i) Given that the useful size of the perturbation (along both the z- and y-directions) is the final boundary layer thickness d, we can estimate that the longitudinal pressure gradient will be non-negligible over a distance of the order of d before and after the leading edge. Everything that happens at distances large compared to d both upstream and downstream of the leading edge, on the other hand, is correctly described by the boundary-layer equations. In particular, although inviscid behaviour continues to dominate over a downstream (and upstream) distance much larger than

d, this behaviour *is* correctly described by the boundary-layer model, because it occurs under negligible pressure gradient, and need not be calculated separately.

(ii) In the leading-edge region of length d, viscous effects are limited to a thin layer of thickness $(dv/U_\infty)^{1/2}$; the inviscid layer above this dominates the flow.

(iii) The vertical displacement of streamlines across this region, calculated from the outer displacement induced by the unperturbed Blasius boundary layer, is of the order of $(dv/U_\infty)^{1/2}$ again, and therefore infinitesimal of order $R^{-1/4}$ with respect to the thickness d of the inviscid layer itself. Thus the upstream and downstream ends of a streamline are asymptotically located at the same vertical coordinate, and the overall evolution of the perturbation along any one streamline can be treated as a jump discontinuity with respect to the long boundary-layer scale L, to within an $O(R^{-1/4})$ error.

(iv) The relationship between physical quantities before and after the discontinuity can be obtained from integrated conservation laws, just as for a shock discontinuity, and from the consideration that, despite an important pressure gradient prevailing in the leading edge region, the total integrated pressure difference must be zero, for in both the upstream and downstream boundary layers pressure is constant in y and equal to the external pressure.

The conclusion drawn from these four considerations in LB is that the longitudinal velocity perturbation δu and the modified longitudinal vorticity perturbation $\delta\xi$, defined by

$$\delta\xi = (u_0\delta w)_y - \mathrm{i}\alpha(u_0\delta v + v_0\delta u)\,, \tag{8}$$

remain continuous across the leading-edge layer.

Therefore, the values of δu and $\delta\xi$ coming from upstream of the leading edge (at $x = 0^-$) can be used as initial conditions for the boundary layer equations at $x = 0^+$. Since upstream of the leading edge $u_0 = 1$ and $v_0 = 0$, the above two quantities can be identified with the longitudinal velocity (or normal vorticity) and longitudinal vorticity perturbations transported by the free stream. Notice that, as v_0 is discontinuous, continuity of δu and $\delta\xi$ implies that either δv or δw must be discontinuous as well. Generally both are.

It follows that the state vector of the perturbation, in § 2 generically denoted $\boldsymbol{f}$, must be seen as composed of the two functions $\delta u(y)$ and $\delta\xi(y)$. It also follows that the natural variables for the backward calculation are the streak receptivity $\bar{u}(x, y)$ and the roll receptivity $\bar{\bar{\xi}}(x, y)$, defined in LB by the property that the scalar product

$$s = \int_0^\infty \left(\bar{u}\delta u + \bar{\bar{\xi}}\delta\xi\right) \mathrm{d}y \tag{9}$$

is constant with x, and therefore takes equal values in the input and output cross-sections. It goes without saying that the boundary-layer equations, and with them their adjoints, do not contain the Reynolds number other than in the scaling of the dependent and independent variables, and only represent the leading term of an expansion of the solution of the Navier–Stokes equations in inverse powers of the Reynolds number.

5. The large-Reynolds-number limit of the input and output energies

The intensity of fluid dynamic instabilities is generally measured by the average change they induce in the kinetic energy of the fluid. In a spatially evolving problem like the present one, the appropriate quantity to represent this change is the integral

of the kinetic energy density over the boundary-layer thickness, i.e.

$$E^{(d)} = \frac{\rho}{4}\int_0^\infty (|\delta u^{(d)}|^2 + |\delta v^{(d)}|^2 + |\delta w^{(d)}|^2)\,\mathrm{d}y^{(d)}, \tag{10}$$

a (d) superscript denoting dimensional quantities, and the cross-products with the base flow having disappeared as an effect of the averaging. When (10) is non-dimensionalized in boundary-layer scaling, it becomes

$$E = \int_0^\infty [|\delta u|^2 + R^{-1}(|\delta v|^2 + |\delta w|^2)]\,\mathrm{d}y \tag{11}$$

and thus contains terms of two different orders in R^{-1}.

The origin of the boundary-layer approximation being in the inner–outer matched asymptotic expansions in inverse powers of the Reynolds number, it is inconsistent to keep both terms of (11) unless the next term of the inner and outer expansion (both of the base flow and of the perturbation) is taken into account in the flow equations at the same time. Therefore, the term $R^{-1}(|\delta v|^2 + |\delta w|^2)$ cannot be retained in the leading boundary-layer approximation of the energy whenever $|\delta u|^2$ is non-zero.

In particular, the optimal-perturbation problem (2) consists of maximizing

$$g = \frac{E_{out}}{E_{in}} = \frac{\left\{\displaystyle\int_0^\infty [|\delta u|^2 + R^{-1}(|\delta v|^2 + |\delta w|^2)]\mathrm{d}y\right\}_{x=x_{out}}}{\left\{\displaystyle\int_0^\infty [|\delta u|^2 + R^{-1}(|\delta v|^2 + |\delta w|^2)]\mathrm{d}y\right\}_{x=x_{in}}} \tag{12}$$

amongst all input perturbations. In doing so we can usefully distinguish between two different types of initial conditions: conditions such that $\delta u_{in} = 0$ and conditions such that the initial δu is different from zero. In fact, in the first case g can be written as

$$g = R\frac{\left\{\displaystyle\int_0^\infty [|\delta u|^2 + R^{-1}(|\delta v|^2 + |\delta w|^2)]\,\mathrm{d}y\right\}_{x=x_{out}}}{\left\{\displaystyle\int_0^\infty [|\delta v|^2 + |\delta w|^2]\,\mathrm{d}y\right\}_{x=x_{in}}} \tag{13}$$

and is $O(R)$, whereas in the second case g is $O(1)$. Clearly, for large enough Reynolds number the gain obtained by initial conditions with $\delta u = 0$ will always exceed the gain obtained by initial conditions with $\delta u \neq 0$, and thus the leading approximation of the optimal condition in the boundary-layer limit of $R \to \infty$ must be sought amongst the perturbations that have $\delta u_{in} = 0$.

At the same time, provided δu_{out} is non-zero (and indeed, we want it to be maximum), we are not allowed to retain $O(R^{-1})$ terms in (13) without at the same time considering higher-order corrections to the boundary-layer equations. Therefore the expression for g simplifies to

$$g = R\frac{\left[\displaystyle\int_0^\infty |\delta u|^2 dy\right]_{x=x_{out}}}{\left\{\displaystyle\int_0^\infty [|\delta v|^2 + |\delta w|^2]\mathrm{d}y\right\}_{x=x_{in}}}. \tag{14}$$

In this form, the expression for g does not contain the Reynolds number other than in the role of a scaling parameter, just as for the boundary-layer equations themselves.

The maximum of (14) constrained over initial conditions such that $\delta u_{in} = 0$ represents the $R \to \infty$ limit of the unconstrained maximum of (12) over all possible initial conditions.

We have thus determined the $\mathbf{Q}_{in}$ and $\mathbf{Q}_{out}$ operators appropriate to the boundary layer model. According to (14), $\mathbf{Q}_{out}$ is a diagonal matrix with unit elements with respect to δu and zero elements with respect to $\delta\xi$, so as to produce the integral of $|\delta u|^2$ from the product $\boldsymbol{f}^* \cdot \mathbf{Q}_{out} \cdot \boldsymbol{f}$. Therefore, in step $\mathbf{Q}_{out}$ of the optimization algorithm we simply set $\bar{\xi}_{out} = 0$ and $\bar{u}_{out} = \delta u^*_{out}$.

On the other side, at the input cross-section, equations (1) require two initial conditions, for the longitudinal velocity perturbation δu and the modified longitudinal vorticity perturbation $\delta\xi$. Once δu_{in} is fixed at zero, the solution will be a functional of $\delta\xi_{in}$ only, and the input energy matrix must be expressed in terms of this quantity.

Upstream of the leading edge, where $u_0 = 1$ and $\delta u = 0$ uniformly in x, the continuity equation (2a) implies that $\delta w = -\delta v_y/(\mathrm{i}\alpha)$. Therefore, the input energy can be expressed as

$$E_{in} = \int_0^\infty (|\delta v|^2 + \alpha^{-2}|\delta v_y|^2)\,\mathrm{d}y = \frac{1}{\alpha^2}\int_0^\infty \delta v^*(\alpha^2\delta v - \delta v_{yy})\,\mathrm{d}y \tag{15}$$

and the streamwise vorticity of (8) as

$$\mathrm{i}\alpha\delta\xi = \alpha^2\delta v - \delta v_{yy}. \tag{16}$$

If now the symbol $\mathbf{D}$ is introduced according to $\mathbf{D} = \alpha^2 - \partial^2/\partial y^2$ (i.e. the opposite of the Fourier-transformed two-dimensional Laplace operator), we can compactly write (15)–(16) as $E_{in} = \alpha^{-2}\delta v^* \cdot \mathbf{D} \cdot \delta v$ and $\mathrm{i}\alpha\delta\xi = \mathbf{D} \cdot \delta v$. As $\mathbf{D}$ is self-adjoint, the expression for the energy as a functional of $\delta\xi$ can be seen to be simply given by

$$E_{in} = \delta\xi^* \cdot \mathbf{D}^{-1} \cdot \mathbf{D} \cdot \mathbf{D}^{-1} \cdot \delta\xi = \delta\xi^* \cdot \mathbf{D}^{-1} \cdot \delta\xi\,. \tag{17}$$

Thus the operation of $\mathbf{Q}_{in}$ consists in applying $\mathbf{D}^{-1}$ to $\delta\xi_{in}$, and the inverse $\mathbf{Q}_{in}^{-1}$ (all that we actually need in the optimization algorithm) consists in applying precisely $\mathbf{D}$ to $\bar{\xi}_{in}$.

We have thus arrived at the definition of the last step in our algorithm, step $\mathbf{Q}_{in}$: once the receptivity $\bar{\xi}_{in}$ at the leading edge is provided by the backward-marching adjoint computation (i.e. $\bar{\boldsymbol{f}}^*_{in} = \mathbf{U}^+ \cdot \bar{\boldsymbol{f}}^*_{out}$, or equivalently $\bar{\boldsymbol{f}}_{in} = \mathbf{U}^T \cdot \bar{\boldsymbol{f}}_{out}$), the new approximation of the initial perturbation (to be used as an initial condition in resuming the loop) is given by $\delta u_{in} = 0$ and $\delta\xi_{in} = \mathbf{D} \cdot \bar{\xi}^*_{in}$. In practice, given (16), we may even more easily set $\delta v_{in} = \mathrm{i}\alpha\bar{\xi}^*_{in}$.

6. Results

As any dependence on the Reynolds number is implicit in the boundary-layer scaling of (1) and (14), the only dimensionless parameters left are the spanwise wavenumber α and the frequency ω of the impinging perturbation. We have, thus, performed a number of computations for different values of α and ω, seeking for each the most amplified initial perturbation and the corresponding induced disturbance at the outlet. We may recall that our inlet ($x_{in} = 0^-$) is the free stream immediately upstream of the leading edge, whereas our outlet ($x_{out} = 1$) is an arbitrary location on the flat plate whose abscissa was chosen as the reference length L (it does not matter whether the plate actually ends at $x^{(d)} = L$ or not, for the boundary-layer equations are parabolic and no upstream influence is felt of whatever happens after x_{out}).

The main results of these computations are contained in figures 1–3. Figure 1

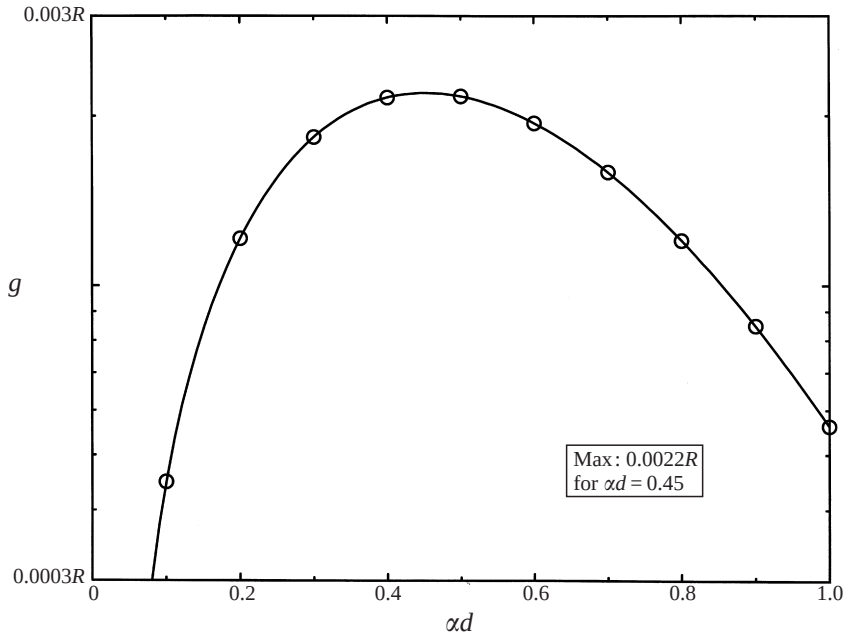

FIGURE 1. Maximum kinetic-energy gain as a function of wavenumber, for zero frequency.

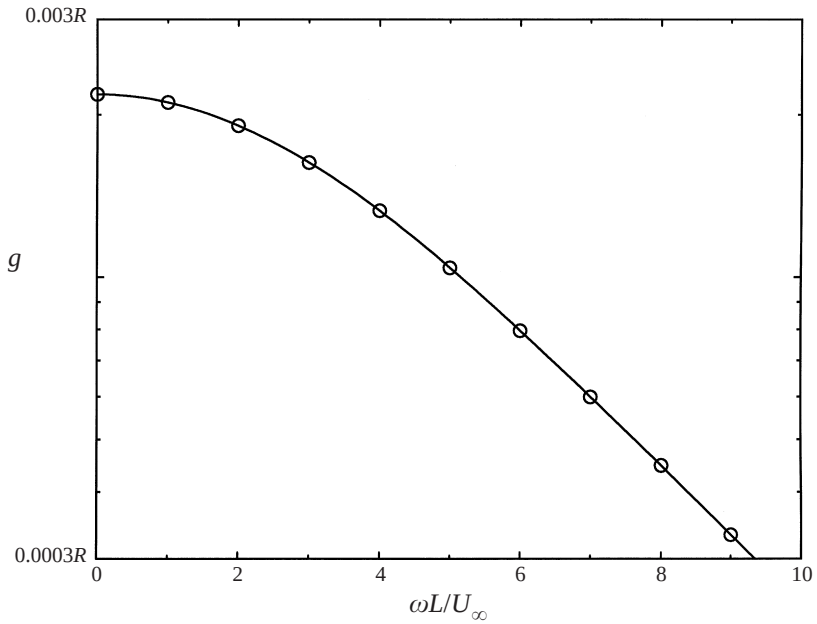

FIGURE 2. Maximum kinetic-energy gain as a function of frequency, for the optimal wavenumber $\alpha d = 0.45$.

displays the curve of maximum amplification as a function of wavenumber α, for zero frequency. A maximally amplified wavenumber $\alpha_{max}^{(d)} = 0.45\,d^{-1}$ (or $0.77\,\delta^{*-1}$, in terms of the displacement thickness $\delta^* = 1.702\,d$) emerges, with a corresponding kinetic-energy gain $g_{max} = 0.0022R = (0.028R_{\delta^*})^2$. Figure 2 displays the curve of

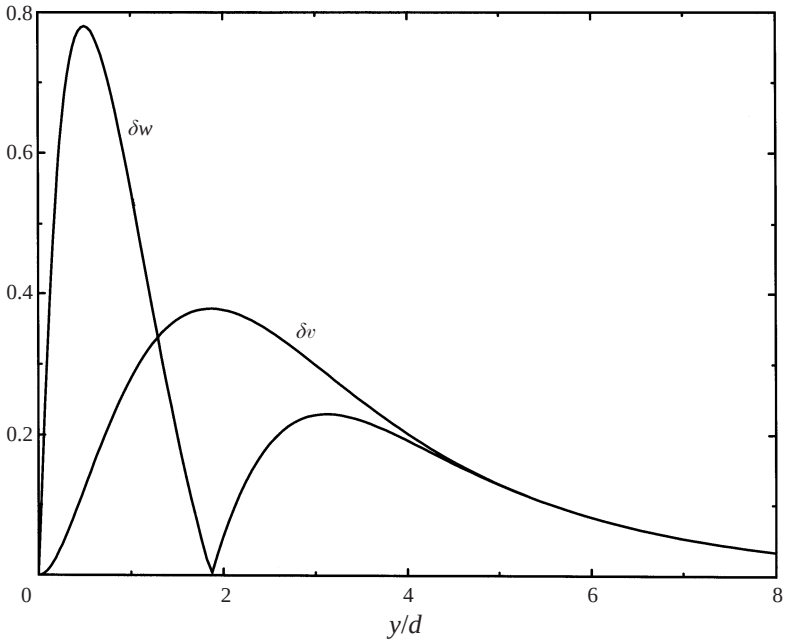

FIGURE 3. Crossflow velocity profiles of the optimal perturbation ($\alpha d = 0.45$, $\omega = 0$).

maximum amplification as a function of ω, for $\alpha = 0.45$. It clearly shows that the maximum occurs for zero frequency, and that perturbations with a dimensionless frequency $\omega = \omega^{(d)}L/U_\infty$ of order unity or less will be preferentially amplified. The δv and δw profiles that constitute an optimal initial perturbation at the wavenumber of maximum amplification are plotted in figure 3. As a side effect of the iteration conditions detailed at the end of the previous section, the initial δv profile plotted in figure 3 also represents the optimal roll receptivity $\bar{\xi}$.

It must be remarked that, if the plot of figure 2 were continued to higher and higher frequencies, it would eventually enter the instability region of classical Tollmien–Schlichting (T–S) waves, and amplification should be expected to rise again (provided the boundary-layer equations (1) were abandoned in favour of a model that also includes the longitudinal pressure gradient, which at high frequency is no longer negligible). In order to estimate where in the spectrum T–S waves and algebraic instabilities are located with respect to each other it can be reckoned, for instance, that the classical neutral threshold of two-dimensional, parallel T–S waves, $R_d = L/d \approx 300$ and $\omega^{(d)}d/U_\infty \approx 0.07$, corresponds to $\omega^{(d)}L/U_\infty \approx 21$, i.e. beyond the end of the plot in figure 2. If it is considered that a substantial amplification of T–S waves requires a further increase in Reynolds number, the algebraic instability and the classical exponential instability can be seen to be quite well separated in frequency.

Figure 4 reports the optimal perturbations for a range of values of α; as may be seen, there is considerable change in the thickness of the various perturbation profiles. In contrast to this behaviour, the final δu profiles, that is the longitudinal-velocity perturbations produced at the outlet when the optimal perturbation is assigned as an initial condition, change very little with α (figure 5). Indeed, they always remain very close to the shape of the small-α similarity solution calculated in L96 (compare figure 2 therein), even when they correspond to a wavenumber which is not small.

Even more interestingly, the final δu profile corresponding to the small-α limit, and

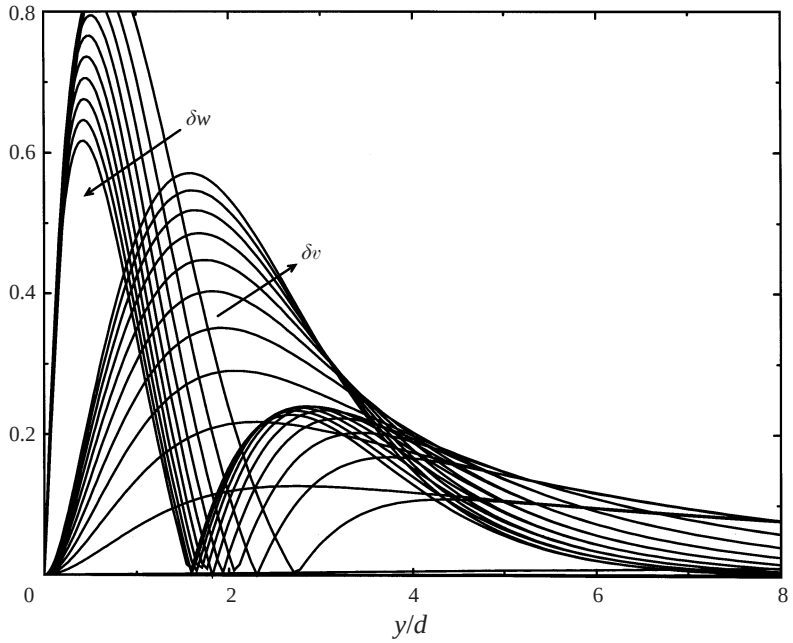

FIGURE 4. Crossflow velocity profiles of the optimal perturbation ($\alpha d = 0.1$–1, $\omega = 0$). The arrow points in the direction of increasing α.

with it all the other profiles plotted in figure 5, are remarkably close to the results of Westin *et al.*'s (1994) experiments, as pointed out to the author by one of the experimenters (P. H. Alfredsson 1996, personal communication). Some of that paper's data (see also Westin 1997) can be seen in figure 6, normalized to unit maximum value and with the optimal-perturbation result superposed. They represent profiles of r.m.s. velocity perturbation measured in a carefully generated flat-plate boundary layer at various longitudinal stations and free-stream velocities corresponding to the Reynolds number R_{δ^*} displayed in the legend. It should be remarked that the experiments were conducted with grid-generated turbulence as excitation, and they agree with the optimization result even if the perturbation applied in the experiment was in no way optimized. (The background turbulence level of 1.5% is the reason why the experimentally produced r.m.s. profiles do not tend to zero for $y \to \infty$ whereas the optimal curve does. Of course, a disturbance exhibiting a non-zero value at infinity cannot be optimal for its energy is infinite.) It may thus be expected that a δu profile similar to this could be found under quite general experimental conditions, even when they are not intentionally tailored to be optimal. Some considerations supporting this expectation are given in Appendix A.

One may also wonder, seeing that the optimal perturbation is characterized by $\delta u_{in} = 0$, whether an initial δu is amplified at all. This question will be addressed in Appendix B.

From the computational point of view, we can report that the convergence of the simple iterative algorithm of § 3 proved very fast for the present problem, giving an accuracy much beyond the truncation errors involved in discretizing the equations after just three or four iterations. The use of more sophisticated iteration strategies was therefore unnecessary.

Indeed, the near universality of the output velocity profile and the quick convergence of the numerical iteration have a common origin in the structure of the singular-value

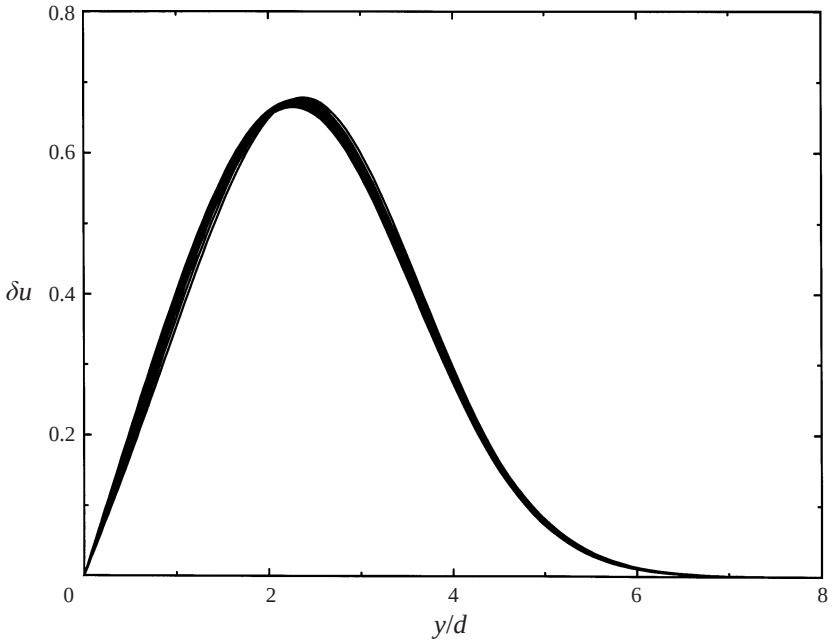

FIGURE 5. Profile of the final longitudinal velocity oscillation induced by an optimal perturbation ($\alpha d = 0.1$–1, $\omega = 0$).

spectrum of the input–output transfer operator; more specifically, both depend on the amount of separation between the first and the other singular values. In fact, the evolution operator $\mathbf{U}$ may always be written in the form of a singular-vector decomposition as

$$\mathbf{U} = \sum_n \sqrt{g_n} \boldsymbol{f}_{out,n} \boldsymbol{f}^*_{in,n} \cdot \mathbf{Q}_{in}, \tag{18}$$

where the input vectors $\boldsymbol{f}_{in,n}$ (eigenvectors of $\mathbf{Q}_{in}^{-1} \cdot \mathbf{U}^+ \cdot \mathbf{Q}_{out} \cdot \mathbf{U}$) are orthonormal with respect to the quadratic form $\mathbf{Q}_{in}$ (i.e. $\boldsymbol{f}^*_{in,m} \cdot \mathbf{Q}_{in} \cdot \boldsymbol{f}_{in,n} = \delta_{m,n}$), and the output vectors $\boldsymbol{f}_{out,n} = g_n^{-1/2} \mathbf{U} \cdot \boldsymbol{f}_{in,n}$ are orthonormal with respect to the quadratic form $\mathbf{Q}_{out}$ (i.e., $\boldsymbol{f}^*_{out,m} \cdot \mathbf{Q}_{out} \cdot \boldsymbol{f}_{out,n} = \delta_{m,n}$). If the singular values are numbered in order of decreasing magnitude, $f_{in,1}$ coincides with the optimal perturbation and $f_{out,1}$ with the corresponding output velocity profile.

From (18) one may read that the operation of $\mathbf{U}$ (encompassing the complete process represented by (1)) is tantamount to expanding the initial condition in the orthonormal basis $\boldsymbol{f}_{in,n}$, replacing $\boldsymbol{f}_{in,n}$ by $\boldsymbol{f}_{out,n}$ for each n, and multiplying each coefficient by $\sqrt{g_n}$. If g_1 is much larger than all the other g_n, it should be clear then that a randomly chosen initial disturbance, having a more or less balanced expansion in the input singular vectors, will tend to produce an output consisting almost entirely of the first singular vector, exactly the same as emerges from an optimal perturbation. In fact, whereas the energies of the eigenvectors of a linear problem are only additive when the problem is self-adjoint, the energies of the singular vectors are always additive; therefore it can be stated in full generality, that if the initial perturbation has a non-negligible fraction of its energy in $f_{in,1}$ (namely, a fraction greater than g_2/g_1), the output perturbation will have most of its energy concentrated in $f_{out,1}$.

In order to obtain the ratio between the first and the second singular value, all that was required was to compute the second eigenvalue of (7). This computation was

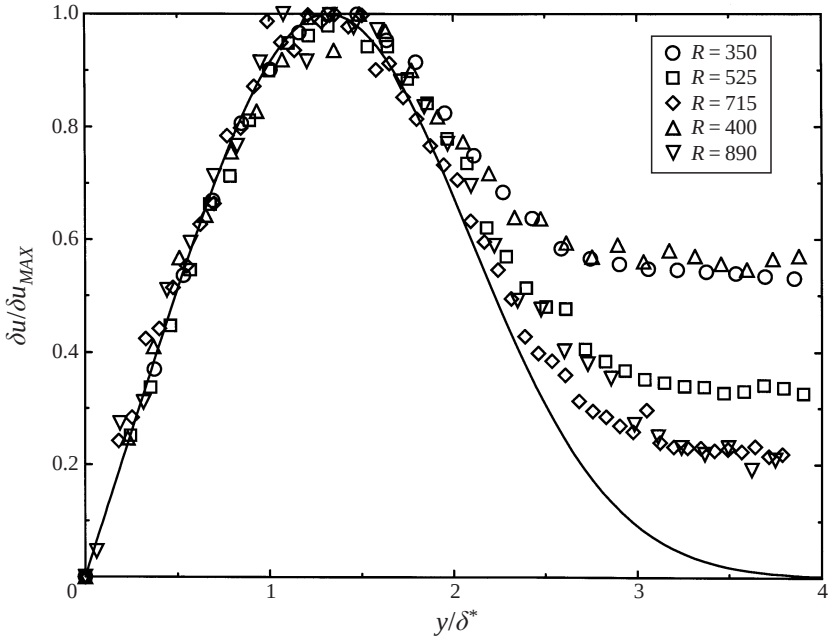

FIGURE 6. Comparison between the δu profile produced by an optimal perturbation and experimental data (from figure 9 of Westin *et al.* 1994, with the authors' permission). Here R is the Reynolds number based on displacement thickness δ^*.

performed by an orthogonalization technique which only required a slight addition to the original program, namely projecting the current vector $\boldsymbol{f}_{in}$ in the hyperplane normal to $\boldsymbol{f}_{in,1}$ before each iteration. The results, shown in figure 7, consistently yield a second singular value almost three orders of magnitude smaller than the first.

7. Conclusions

For a long time the appearance of streamwise streaks as an instability has only been tied to the presence of centrifugal forces in curved flows. Despite the experimental evidence indicating the frequent occurrence of streamwise streaks in pre-transitional flow past straight walls, a theoretical explanation of the linear amplification mechanism of such streaks was missing; therefore their presence (leading to the so-called 'bypass transition') was typically ascribed to an unspecified 'direct nonlinear mechanism' triggered by large values of free-stream disturbances.

Whereas it is true that only in the presence of centrifugal forces do streamwise streaks receive exponential amplification, the scientific community has now realized that the transient amplification allowed by the non-selfadjoint character of the equations of fluid dynamics can produce important energy gains, of the right order of magnitude to explain the linear growth of initially small disturbances up to the point where they can excite nonlinear interactions and eventually cause transition. Perturbations produced in this way are driven by the lift-up phenomenon, that is by the continued accumulation over time (or downstream distance) of longitudinal-velocity differences arising from slow convection in the transverse plane. This mechanism tends to give these perturbations their characteristic aspect of elongated streaks, with a relatively fast oscillation in the spanwise direction and a much slower (in the ideal case, absent) oscillation in the longitudinal direction and in time. They are,

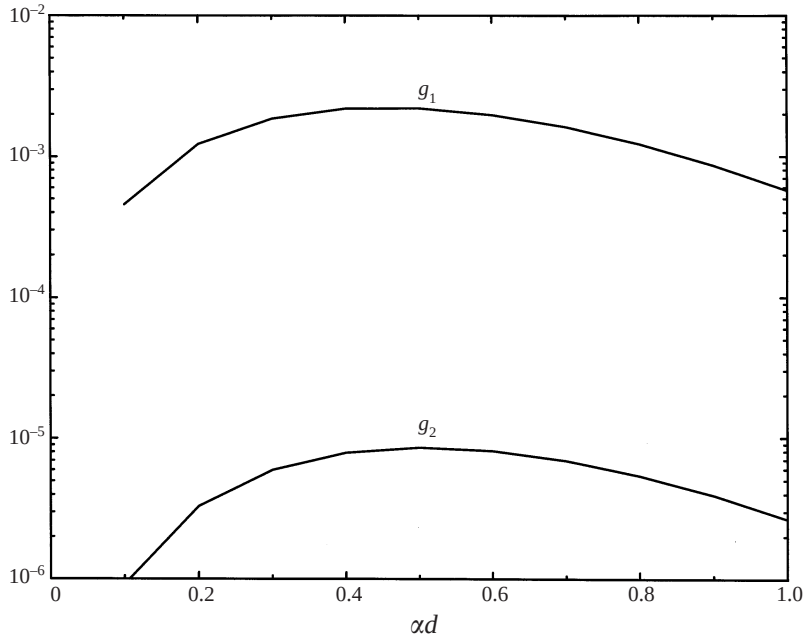

FIGURE 7. First and second singular values of the evolution operator as functions of wavenumber.

therefore, very different from the classical Tollmien–Schlichting waves, which in their first-destabilization range are characterized by a fast oscillation in the longitudinal direction and in time, and a slow (in the ideal case, absent) oscillation in the spanwise direction. Rather, algebraic instabilities of the boundary layer tend to have an appearance quite similar to Görtler vortices, with which they share the basic mathematical model. The only difference is that on a curved plate centrifugal forces create a feedback from the streamwise streaks onto the crossflow vortices, thus making the amplification of Görtler instabilities exponential.

Although the existence of algebraic growth in a boundary layer and its qualitative dependence on the Reynolds number could certainly be inferred from previous theories and computations of the algebraic growth in a parallel flow, this paper has given the first quantitative determination of the maximum amplification factor achievable through this mechanism, and of the corresponding spanwise wavenumber. The maximum amplification factor, $0.0022R$, translates into an energy amplification of 220–2200 (amplitude amplification of 15–50) in the 10^5–10^6 Reynolds-number range where bypass transition is likely to be observed, thus potentially explaining the growth of external disturbances in the 1–5% range to levels where they can trigger transition. The typical spanwise wavenumber of $0.45d^{-1}$ is about half of the typical wavenumber of Görtler vortices, evidently because the larger amplification of the latter can more easily withstand the viscous damping associated with a faster spanwise oscillation. It remains, anyway, near enough to the typical wavenumber of Görtler vortices to corroborate a common explanation of both through the lift-up effect. In addition, just as for Görtler vortices, the frequency of maximum amplification is zero. Of course, in both cases this is not to be understood in the sense that only steady Görtler vortices and streaks are to be expected in practice, but in the sense that observed frequencies will be in the range where the amplification is not too different from its value at zero, according to figure 2. From a theoretical viewpoint, however, the fact

that the amplification range is centred at zero frequency makes the (easier) steady case particularly interesting to study.

A separate consideration is required by the fact that the velocity profile assumed by the streak appears to be almost insensitive both to the wavenumber and frequency (within a reasonable range) and to the shape of the initial perturbation. Indeed, it was observed by G. I. Taylor as early as 1939 that the experimentally measured r.m.s. perturbation profiles of transitional flows tended to assume the typical shape with a single maximum that would be expected from a small modulation in boundary-layer thickness, rather than the very different shape with two maxima which is characteristic of Tollmien–Schlichting waves.† This is also borne out by the present comparison of the theoretical streak profile with the experimental results of Westin *et al.* (1994). In fact, a concordance between the theoretical and experimental velocity profiles was not even to be expected, if it was considered that the experiments were performed with homogeneous grid turbulence and not with optimal perturbations as initial conditions. A mathematical, objective, explanation for this concordance has been given at the end of the previous section through the spectral properties of the evolution matrix, thus making it clear that the shape of the streak always tends to be attracted towards the shape of the optimal perturbation, even when the initial perturbation is relatively far from optimal. A more physical, but also more debatable, conjecture of loose coupling between the different equations of the model is given in Appendix A. One point in favour of this conjecture is that it can also explain why the universal shape that the streak tends to assume is very near to a simple thickness modulation, just as empirically observed by G. I. Taylor and later experimenters.

Finally it should be mentioned that, while this paper was being revised, a number of related approaches have been presented at conferences and/or in journals.

In particular, Andersson *et al.* (1998*a*, *b*, *c*, 1999*a*, *b*, *c*, *d*) have calculated the optimal perturbations of a flat-plate boundary layer by a similar backtracking optimization technique, the main difference being that their energy ratio is defined as in (12) rather than in the Reynolds-independent form of (14), whereas their mathematical model is still constituted by the boundary-layer equations. They thus obtained steady amplification spectra in which dependence on the Reynolds number is accounted for in the definition of energy but not in the model equations. Their data confirm that the result of optimizing (12) does indeed converge to the result of optimizing (14) for $R \to \infty$, and moreover that the Reynolds-independent limit is for all practical purposes attained in the interesting range of $R \approx 10^5$–10^6; however, they cannot be relied upon to give the true Reynolds-number dependence below this range, because the deviation of the optimal gain from its asymptotic value is $O(1/R)$, and not all $O(1/R)$ effects are taken into account. It is also of some concern that the leading-edge region is given hardly any consideration by Andersson *et al.*, who claim continuity of their optimization results when x tends to zero from the right, but then in the computation set $v_0 = 0$ for $x = 0$, disregarding the fact that the limit of the normal velocity of Blasius flow when x tends to zero from the right is infinity. Therefore, although the gain figures presented are to graphical accuracy the same, here they can be interpreted as the ratio of final energy to energy of free-stream perturbations measured just upstream of the leading edge whereas in Andersson *et al.* they cannot.

† On p. 305 of Taylor (1939) we read: "[From recent measurements in the non turbulent layer near a flat plate in the Cambridge tunnel] it will be seen that the fluctuations are confined entirely to the boundary layer, $\sqrt{\overline{u^2}}$ falling to the general level of turbulence in the tunnel immediately outside the layer. This fact combined with the comparative slowness of the fluctuations makes it appear probable that they are simply fluctuations in boundary layer thickness."

In addition, higher singular values and the universality of the output streak profile are only discussed in the present paper; frequency dependence was added during the first revision to corroborate the former assumption that maximum gain is obtained for zero frequency and determine the useful frequency range of near-optimal amplification. On the other hand, only the papers by Andersson *et al.* present an empirical correlation of algebraic growth for transition-prediction purposes.

Cossu, Costa & Chomaz (1998) optimized the energy growth of steady Görtler vortices, including the flat-plate boundary layer as the particular case of zero curvature, by first determining a matrix representation of the input–output transfer operator $\mathbf{U}$. Their results are not directly comparable with ours because they adopted still another definition of the energy density, the sum of the square moduli of all three dimensionless velocity components, disregarding the fact that in a boundary layer the longitudinal and transverse velocity components are made dimensionless with respect to different reference values.

Tumin (1998) reconsidered the previous calculation by Crow (1966) of the linear growth induced in the δu-component of velocity by a spanwise oscillation of small α of the free stream, and extended it to unsteady perturbations. The effect studied in 1966 by Crow himself, of a growing streak being induced by a weak and slow spanwise modulation of the direction of the outer stream, is a cunning limiting case of (1) in which the problem can be solved analytically. Indeed, when the spanwise wavelength and normal thickness of the perturbation are both large compared to the boundary layer thickness, $\delta\xi$ becomes independent of x and δu linear in x. For infinite thickness Crow's problem is obtained, but at the price of an infinite driving energy. If the energy of the driving vortex is not an issue, the amplitude of the streak grows linearly from zero. On the other hand, if the energy of the vortex is included in the budget, the ratio of output to input energy increases with the vortex becoming of shorter wavelength and moving closer and closer to the wall, where Crow's limit is lost, and the maximum is eventually attained for the optimal perturbation computed here. Interestingly, the output velocity profile only changes by a hardly visible amount in the process.

This work was supported by the Italian Ministry of University and Research and by the ERCOFTAC Leonhard Euler Research Centre at the Ecole Politéchnique Fédérale de Lausanne (EPFL), Switzerland. A. Bottaro and P. A. Monkewitz of EPFL and P. H. Alfredsson of the Royal Institute of Technology (KTH), Sweden, are thanked for useful comments and discussion. P. H. Alfredsson and K. J. A. Westin of KTH are thanked for making their experimental data available for comparison, and for pointing out the reference to G. I. Taylor (1939). An oral presentation of the contents of this paper was given at the 3rd EUROMECH Fluid Mechanics Conference, Göttingen, 15–18 Sept. 1997.

Appendix A. A conjecture explaining why the final velocity profile is so repeatable

As shown at the end of §6, the optimal output velocity profile of figure 5 not only tends to emerge from the optimal initial perturbation, but also from a generic initial perturbation not orthogonal to it. Incidentally, this also explains why the first (and second) mode of the small-α similarity solution calculated in L96 fall very near to each other and to the optimal profile itself. (Indeed, it is the similarity profile that was observed to agree with experimental data by P. H. Alfredsson; the optimal

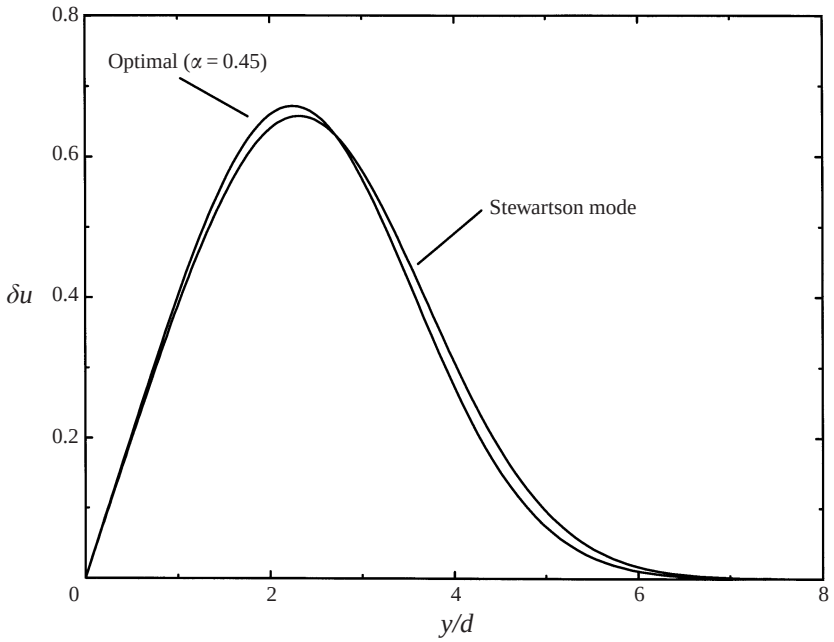

FIGURE 8. Comparison between the δu profile produced by an optimal perturbation and the Stewartson mode.

perturbation profile was not yet available at that time.) While all of this is fortunate, it may also be a hint of an even more elementary mechanism at work. This Appendix aims at presenting a candidate for the role of such mechanism.

We see a revealing clue in still another velocity profile that looks very much like all of the above: the first mode in the sequence described by Libby & Fox (1964) (see also §2 of L96) of similarity solutions to the two-dimensional linearized boundary-layer equations (i.e. (1) with $\alpha = 0$ and $\delta w = 0$). This mode, plotted in figure 8 together with the present optimization result, has an analytical expression (due to Stewartson 1957) simply given by $\delta u = y u_{0,y}$, Blasius' solution being denoted by u_0. It should be noted that this is the same perturbation profile that would follow from an infinitesimal modulation of boundary-layer thickness. In fact, if the Blasius velocity profile is written as $u = u_0[y/h(x)]$ and the boundary-layer thickness h is given a small variation δh, the velocity increment $\delta u = u - u_0$ turns out to be proportional to the same Stewartson mode: $\delta u = -(\delta h/h) y u_{0,y}$. (Indeed, this is more or less how Stewartson discovered his exact solution of the steady, two-dimensional perturbation equations.)

We thus propose the following conjecture to explain the strong resemblance between the δu profile obtained from an optimal perturbation and the one generated by quite different initial perturbations (such as those presumably present in the experiments): *the Stewartson mode of the Libby & Fox sequence is a strong enough attractor to bring near to itself the velocity profile under most* (*reasonably smooth*) *initial conditions.*

How such an attraction can take place may be seen in its simplest form in the case of the small-α three-dimensional modes studied in L96. According to equations (L96.7) (by which we mean equations (7) of L96), the three-dimensional modes consist of driven solutions of the Libby and Fox equations (L96.10), where the driving is provided by free eigensolutions of a separate equation for δw (L96.9). Since the

Libby & Fox modes form a complete set, orthogonal with respect to a suitable weight function, it is always possible to represent the solution of (L96.7a, b) as a superposition of modes, namely

$$\delta u = \sum_{k=1}^{\infty} a_k(x) N_k'(y/x^{1/2}) \tag{A 1}$$

(in the symbolism of L96), where the coefficient a_k obeys the ordinary differential equation:

$$\frac{\mathrm{d}a_k}{\mathrm{d}x} + r_k x^{-1} a_k = \int_0^{\infty} H_k(\eta) F_0'^2(\eta) \int_0^{\eta} \mathrm{i}\alpha \delta w(x,\ x^{1/2}\eta_1)\, \mathrm{d}\eta_1 \mathrm{d}\eta. \tag{A 2}$$

In the case where δw represents the jth eigensolution of (L96.9), proportional to x^{-s_j}, the relative amplitude of the different coefficients a_k will depend both on the affinity between the wall-normal profile of the spanwise velocity perturbation δw and the shape of the kth mode (as expressed by the integral on the right-hand side of (A 2)), and on the proximity of exponents $s_j - 1$ and r_k (i.e. the degree of resonance with the left-hand side). In practice, for the first two modes $s_1 - 1$ (i.e. -0.213) and $s_2 - 1$ (i.e. 0.694) are closer to $r_1 = 1$ than to any other Libby & Fox eigenvalue, and the component a_1 prevails. Thus the fact that the first two modes exhibit the same general appearance as the Stewartson mode can be explained. In addition the resonance is even stronger for the second than for the first mode, and therefore, as visible in figure 2 of L96, the second mode has a higher amplitude than the first.

The same mechanism may be expected to operate even when, for α not being small, the spanwise perturbation δw is not independent of δu but is coupled to it by pressure. Equations (1a, b) can still be formally solved and transformed into (A 2), and as long as the variation of δw with x is slow enough the resonance mechanism will make the Stewartson mode prevail in the modal expansion of δu and leave its imprint in the final shape of the velocity profile.

As every z-dependent perturbation that turns into the Stewartson disturbance profile produces only a z-dependent modulation of the *boundary-layer thickness h*, we conclude that the initial linear effect of an infinitesimal longitudinal vortex on the Blasius boundary layer may be expected to almost always produce a simple thickness modulation.

Appendix B. Are streak-only perturbations never amplified?

As was recalled in § 4 and explained in more detail in LB, the three-dimensional boundary layer equations require two initial conditions, one for δu and one for $\delta\xi$ of (8), at $x = x_{in}$, and none at $x = x_{out}$. The qualitative conclusion that $\delta\xi$ (roll) perturbations are amplified much more than δu (streak) ones comes quite simply from their different scaling: a $\delta\xi$ of order unity in boundary-layer variables is actually a small perturbation of order $R^{-1/2}$, and produces a δu of order unity at the outlet cross-section with an $O(R)$ gain in energy; on the other hand a δu of order unity produces an output δu of order unity again (actually a reduced one).

There are two independent deductions one can draw from this observation: one is that the maximally amplified perturbation is a $\delta\xi$-only perturbation, as was shown in § 5 and calculated in § 6; the other is that a δu-only perturbation is not amplified at all. However, these two statements are not quite on the same footing. In fact, whereas a maximum is relatively insensitive to structural perturbations of the problem, and

therefore the conclusion that a $\delta\xi$ perturbation is maximally amplified is relatively robust, a zero can be altered by even a slight modification of the model, and therefore care is needed with the second claim. In particular, it is quite clear that even a small coupling from the initial δu into the initial $\delta\xi$ can make the former amplified, provided only that the coupling is larger than $R^{-1/2}$. Since the approximation of replacing the leading-edge region by a leap discontinuity is only valid to $O(R^{-1/4})$, such a coupling cannot be excluded.

Damped perturbations of course do exist for a linear problem with both large and small singular values, at whatever order of approximation. All that the above means is that the damped perturbation, at a higher order of approximation, will not be a δu-only perturbation but the combination of a δu-profile with a suitable, $O(R^{-1/4})$, $\delta\xi$-profile. Since a δu perturbation is equivalent to a normal vorticity perturbation, another way to see the same effect is that the damped vorticity perturbation, instead of being exactly normal to the wall, will be rotated by an $O(R^{-1/4})$ angle. By the same token, the maximally amplified perturbation may also be rotated by an $O(R^{-1/4})$ angle from its leading-order exactly longitudinal direction, but with only an imperceptible change in the corresponding amplification. All this does not modify the fact that a randomly oriented initial perturbation has an overwhelming probability of containing an $O(1)$ fraction of the maximally amplified component.

A substantial amplification of δu perturbations was indeed obtained by Goldstein, Leib & Cowley (1992), who studied the effect of δu-only perturbations of zero frequency on a flat plate with a rounded leading edge. A crucial, though perhaps underemphasized, starting assumption of their paper is that their plate has a non-zero thickness of the same order of magnitude as the spanwise wavelength of the oncoming perturbation, which is to say of order d. This changes the normal displacement induced in the inviscid stream from $O(dv/U_\infty)^{1/2}$ to $O(d)$, and consequently makes the coupling of δu with $\delta\xi$ perturbations $O(1)$ rather than $O(R^{-1/4})$. Indeed, in the limit of a very blunt edge which can locally be described as a flat plate normal to the stream, quite clearly vorticity perturbations oriented normal to the free stream become parallel to the surface and vice versa.

It is thus not inconsistent with the present findings that Goldstein *et al.* calculated a sizeable amplification of δu-only perturbations (without even trying to optimize them), nor that they had to actually solve the inviscid-region equations (in terms of Lighthill's drift function) in order to do so. However, it does indicate that the optimal perturbations calculated in the present paper might only apply for very thin plates, and that for thick plates the optimal may have to be determined by using the Lighthill drift technique in order to connect the initial perturbation at $x = 0^+$ with the free-stream perturbation prevailing at $x = 0^-$.

REFERENCES

ANDERSSON, P., BERGGREN, M. & HENNINGSON, D. S. 1998*a*, Optimal disturbances in boundary layers. *Proc. AFOSR Workshop on Optimal Design and Control, Arlington VA, USA, 30 Sept.–3 Oct. 1997* (ed. J. T. Borggaard, J. Burns, E. Cliff & S. Schreck) Birkhauser, Boston.

ANDERSSON, P., BERGGREN, M. & HENNINGSON, D. S. 1998*b* Optimal three-dimensional perturbations in the Blasius boundary layer. *7th European Turbulence Conference, Saint Jean Cap Ferrat, France, 30 June–3 July.*

ANDERSSON, P., BERGGREN, M. & HENNINGSON, D. S. 1998*c* Optimal three-dimensional perturbations in the Blasius boundary layer. *EUROMECH 380 Colloquium on Laminar–Turbulent Transition Mechanisms and Prediction, Göttingen, Germany, 14–17 Sept.*

Andersson, P., Berggren, M. & Henningson, D. S. 1999*a* Optimal disturbances and bypass transition in boundary layers. *Phys. Fluids* **11**, 134–150.

Andersson, P., Berggren, M. & Henningson, D. S. 1999*b* Optimal three-dimensional perturbations in the Blasius boundary layer. *COST/ERCOFTAC Transition Modelling SIG Workshop, Cambridge, UK, 25–26 Mar.*

Andersson, P., Berggren, M. & Henningson, D. S. 1999*c* Optimal three-dimensional perturbations in the Blasius boundary layer. *ERCOFTAC Workshop on Adjoint Methods, Toulouse, France, 21–23 June.*

Andersson, P., Berggren, M. & Henningson, D. S. 1999*d* Optimal three-dimensional perturbations in the Blasius boundary layer. *IUTAM Symposium on Laminar–Turbulent Transition, Sedona AZ, USA, 13–17 Sept.*

Baggett, J. S., Driscoll, T. A. & Trefethen, L. N. 1995 A mostly linear model of transition to turbulence. *Phys. Fluids* **7**, 833–838.

Baggett, J. S. & Trefethen, L. N. 1997 Low-dimensional models of subcritical transition to turbulence. *Phys. Fluids* **9**, 1043–1053.

Boberg, L. & Brosa, U. 1988 Onset of turbulence in a pipe. *Z. Natursforschung* **43a**, 697–726.

Butler, K. M. & Farrell, B. F. 1992 Three-dimensional optimal perturbations in viscous shear flow. *Phys. Fluids* A **4**, 1637–1650.

Cossu, C., Costa, M. & Chomaz, J. M. 1998 Maximum spatial growth of Görtler vortices. *EUROMECH 380 Colloquium on Laminar–Turbulent Transition Mechanisms and Prediction, Göttingen, 14–17 Sept.*

Crow, S. C. 1966 The spanwise perturbations of two-dimensional boundary layers. *J. Fluid Mech.* **24**, 153–164.

Ellingsen, T. & Palm, E. 1975 Stability of linear flow. *Phys. Fluids* **18**, 487–488.

Gebhardt, T. & Grossmann, F. 1994 Chaos transition despite linear stability. *Phys. Rev.* E **50**, 3705–3711.

Goldstein, M. E., Leib, S. J. & Cowley, S. J. 1992 Distortion of a flat-plate boundary layer by free-stream vorticity normal to the plate. *J. Fluid Mech.* **237**, 231–260.

Gustavsson, L. H. 1991 Energy growth of three-dimensional disturbances in plane Poiseuille flow. *J. Fluid Mech.* **224**, 241–260.

Hamilton, J. M., Kim, J. & Waleffe, F. 1995 Regeneration mechanisms of near-wall turbulent structures. *J. Fluid Mech.* **287**, 317–348.

Henningson, D. S., Lundbladh, A. & Johansson A. V. 1993 A mechanism for bypass transition from localized disturbances in wall-bounded shear flows. *J. Fluid Mech.* **250**, 169–207.

Hultgren, L. S. & Gustavsson, L. H. 1981 Algebraic growth of disturbances in a laminar boundary layer. *Phys. Fluids* **24**, 1000–1004.

Klebanoff, P. S., Tidstrom, K. D. & Sargent, L. M. 1962 The three-dimensional nature of boundary-layer instability. *J. Fluid Mech.* **12**, 1–34.

Landahl, M. T. 1980 A note on an algebraic instability of inviscid parallel shear flows. *J. Fluid Mech.* **98**, 243–251.

Libby, P. A. & Fox, H. 1964 Some perturbation solutions in laminar boundary-layer theory. *J. Fluid Mech.* **17**, 433–449.

Luchini, P. 1996 Reynolds-number independent instability of the boundary layer over a flat surface. *J. Fluid Mech.* **327**, 101–115 (referred to herein as L96).

Luchini, P. & Bottaro, A. 1996 Görtler vortices: a backward-in-time approach to the receptivity problem. *49th Annual Meeting of the American Physical Society – Division of Fluid Dynamics, Syracuse, N.Y., 24–26 Nov. 1996.* Abstract in *Bull. Am. Phys. Soc.* **41**, 1788 (referred to herein as LB).

Luchini, P. & Bottaro, A. 1998 Görtler vortices: a backward-in-time approach to the receptivity problem. *J. Fluid Mech.* **363**, 1–23 (referred to herein as LB).

Lundbladh, A. & Johansson A.V. 1991 Direct simulation of turbulent spots in plane Couette flow. *J. Fluid Mech.* **229**, 499–516.

Morkovin, M. V. 1968 Critical evaluation of transition from laminar to turbulent shear layer with emphasis on hypersonically travelling bodies. *AFFDL Tech. Rep.* 68–149.

Morkovin, M. V. 1984 Bypass transition to turbulence and research desiderata. In *Transition in Turbines*, pp. 161–204. NASA Conf. Pub. 2386.

Morkovin, M. V. & Reshotko, E. 1990 Dialogue on progress and issues in stability and transition research. In *Laminar-Turbulent Transition* (ed. D. Arnal & R. Michel), pp. 3–29. Springer.

Reddy, S. C. & Henningson, D. S. 1993 Energy growth in viscous channel flow. *J. Fluid Mech.* **252**, 57–70.

Stewartson, K. 1957 On asymptotic expansion in the theory of boundary layer. *J. Math. Phys.* **36**, 137.

Taylor, G. I. 1939 Some recent developments in the study of turbulence. *Proc. Fifth Intl Cong. for Applied Mechanics, Cambridge, MA, USA, Sept. 12–16, 1938* (ed. J. P. den Hartog & H. Peters), pp. 294–310. Wiley.

Ting, L. 1965 On the initial conditions for boundary layer equations. *J. Math. Phys.* **44**, 353.

Trefethen, L. N., Trefethen, A. E., Reddy, S. C. & Driscoll, T. A. 1993 Hydrodynamic stability without eigenvalues. *Science* **261**, 578–584.

Tumin, A. 1998 A model of the Blasius boundary layer response to free-stream vorticity. *EUROMECH 380 Colloquium on Laminar–Turbulent Transition Mechanisms and Prediction, Göttingen, 14–17 Sept.*

Westin, K. J. A. 1997 Laminar-turbulent boundary layer transition influenced by free stream turbulence. Doctoral thesis, Department of Mechanics, Royal Institute of Technology, Stockholm, Sweden.

Westin, K. J. A., Boiko, A. V., Klingmann, B. G. B., Kozlov, V. V. & Alfredsson, P. H. 1994 Experiments in a boundary layer subjected to free stream turbulence. Part 1. Boundary layer structure and receptivity. *J. Fluid Mech.* **281**, 193–218.